JOURNAL OF MATERIALS SCIENCE 30 (1995) 2390–2400

Microstructural modelling of grain-boundary stresses in Alloy 600

K. J. KOZACZEK
Oak Ridge National Laboratory, Oak Ridge, TN 37831, USA
B. G. PETROVIC, C. O. RUUD, S. K. KURTZ
The Pennsylvania State University, University Park, PA 16802, USA
A.R. McILREE
Electric Power Research Institute, Palo Alto, CA 94304, USA

The stress distribution in a random polycrystalline material (Alloy 600) was studied using a topologically correct microstructural model. The distributions of von Mises and hydrostatic stresses, which could be important factors when studying the intergranular stress corrosion cracking, at the grain vertices were analysed as a function of microstructure, grain orientations and loading conditions. The grain size, shape, and orientation had a more pronounced effect on stress distribution than the loading conditions. The stress concentration factor was higher for hydrostatic stress (1.7) than for von Mises stress (1.5). Hydrostatic stress showed more pronounced dependence on the disorientation angle than von Mises stress. The observed stress concentration is high enough to cause localized plastic microdeformation, even when the polycrystalline aggregate is in the macroscopic elastic regime. The modelling of stresses and strains in polycrystalline materials can identify the microstructures (grain-size distributions, texture) intrinsically susceptible to stress/strain concentrations and justify the correctness of applied stress state during the stress corrosion cracking tests.

1. Introduction

Intergranular cracks found on primary and secondary sides of steam generators with Alloy 600 (approximately 75% Ni, 15% Cr, 10% Fe, wt %) tubing and other Alloy 600 components such as control rod drive and pressurizer nozzles, are attributed to intergranular stress corrosion cracking (IGSCC). The process of intergranular stress corrosion in metal alloys is controlled by a combination of corrosive environment, applied (and/or residual) stress, and a susceptible microstructure. The microstructural characteristics often cited as affecting the susceptibility of nickel alloys to IGSCC in high-temperature water are intergranular [1–14] and intragranular [2] carbides, grain-boundary chromium depletion [1, 3, 5, 7, 8, 10–12, 14–16], impurity segregation [1–3, 8, 10–13, 17–19], grain size [10, 20], texture and cold work [10, 20, 21]. The susceptibility to corrosion and stress corrosion cracking can also depend on the grain-boundary misorientation [22–28].

The role of stress in the process of crack initiation and propagation is not fully understood, mostly due to the fact that there is no clear understanding of mechanisms of crack initiation and propagation. There is, however, experimental evidence that intergranular cracks in Alloy 600 primarily initiate and propagate at locations where a complex state of stress exists [20], regardless of the type of loading (static or cyclic) [29]. Historically, IGSCC has been studied using test specimens whose results are a combination of crack initiation and growth. There exist several theories explaining the experimental observations in terms of environment chemistry, microstructure and stress/strain state: film rupture–slip dissolution (oxidation) process [16, 30–36], hydrogen-assisted cracking [20, 37, 38], internal oxidation [39], and composite mechanisms. The experimental evidence shows that there is a stress threshold for cracking which depends on the proposed stress corrosion cracking (SCC) mechanism [7, 40, 41]. Systems with thick, brittle oxide films would be sensitive to the maximum principal stress; the failure criteria for systems with ductile passive films would involve the total strain energy (von Mises equivalent stress) [41]. The mechanisms involving the formation of intergranular bubbles can be sensitive to the hydrostatic pressure in the material [41]. There is, however, no published experimental evidence that the mechanisms governing the crack initiation and propagation are the same; one can assume that the slip-related mechanism would be controlled by the deviatoric stresses (e.g. von Mises equivalent stress) which are responsible for material shearing, and the rupture-type mechanism (no plastic deformation) would depend on the hydrostatic stresses. The current understanding of the role of stress in crack initiation is such that the crack initiates at sites where a local stress concentration exists [20, 28, 32]. Grain boundaries, slip steps, and corrosion pits act as stress raisers [28, 32]. Localized plastic deformation leads to film rupture and to the nucleation of a crack

0022–2461

[28]. Also, it is believed that selective corrosive attack is strongly correlated with the non-uniform distribution of microstrains [9]. In order to deform material microplastically, the local stress must exceed the yielding stress. A polycrystal is an aggregate of randomly (or preferably) oriented grains and under applied (and/or residual) stress inhomogeneous stress and strain distributions exist [42–45]. The local stress state is a superposition of three "types" of stresses [42, 46]: (1) the homogeneous stress state, which is averaged over the volume of many crystallites (called "macrostress"), (2) the inhomogeneous stress which varies within a crystallite due to its interactions with the neighbouring grains ("microstress"), and (3) stress variations due to lattice defects (dislocations, vacancies, precipitates, etc.) called "sub-microstress".

The stress fields caused by dislocation pile-ups can be calculated analytically for some types of dislocation arrays [47–50]. The magnitude of these stresses can be high enough to produce the secondary slip (stress relaxation) in fcc crystals over distances of the order of the pile-up length [49] provided that the dislocation density is sufficiently high. The magnitude of "sub-microstresses" is a function (among other factors) of dislocation density and local microstress [48].

The microstress is the difference between the average stress in a particular crystallite and the average stress in the polycrystalline aggregate. The magnitude of the principal stresses within the crystallite depends on its orientation with respect to the applied stress tensor and the elastic interactions with the neighbouring grains. These elastic interactions are functions of the degree of elastic anisotropy, the misorientation angles between the adjacent grains (texture-dependent) and the number of neighbouring grains.

Finally, the macroscopic stress is a superposition of residual stresses (mostly due to manufacturing processes) and applied stresses. It is generally accepted that on the surface there is a plane biaxial state of stress, which becomes triaxial with the crack initiation. The role of stress state on crack initiation is not clear; many SCC tests in high-temperature water environments have resorted to specimens with complex stress states (i.e. reversed U-bends) to reduce test times. The influence of biaxial, triaxial, and cyclic stresses is yet to be determined [41].

It has been recognized that the grain-boundary misorientation (relative misorientation between adjacent grains) has an influence on corrosion [23–26] and intergranular stress corrosion cracking [51]. A recent study [22] showed that for Alloy 600 the coincident site lattice boundaries (CSLBs have the misorientation where the two lattices of the adjacent grains have some coincident points) are more resistant to IGSCC than general high-angle boundaries (GHABs are boundaries with the misorientation angle greater than 15°) regardless of the test environment. It was also suggested that the grain-boundary character distribution affects the crack initiation more than it affects the crack propagation. If one is to explain the mechanistic aspects of crack initiation in terms of localized plasticity or rupture-type damage, it is necessary to study the stress concentration as a function of grain-boundary character distribution (i.e. low-angle grain boundaries versus GHABs and CSLBs). The proportion of CSLBs for a random polycrystal is relatively small [52] (less than 10%). However, if the preferred orientation (texture) is present in the material, the proportion of CSLBs can be drastically enhanced [52–54]. It has been reported that for Ni–16 Cr–9 Fe alloy the proportions of CSLBs could be increased up to 51% through sequential tensile deformation and heat treatments [22].

This study is concerned with the distribution of stresses between individual randomly oriented crystallites in a "pure" microstructure (i.e. without impurities of precipitates) of a single-phase alloy. The local concentrations of stresses at vertices in three-dimensional microstructures (grain-boundary triple points at the surface in two-dimensional case) were studied as a function of misorientation angles and the state of applied stress. The "pure" microstructure was selected for this study in order to determine the effect of the "intrinsic" properties of the microstructure (i.e. single-crystal elastic anisotropy and grain topology) on the stress distribution.

2. Model of a polycrystalline aggregate

2.1. Three-dimensional Poisson–Voronoi tessellation

A three-dimensional microstructure was simulated using a Poisson–Voronoi tessellation described in detail elsewhere [55]. The Poisson–Voronoi tessellation represents the microstructure which results from the growth of crystals from nuclei randomly distributed in a three-dimensional space and which appear simultaneously in time. The grain-growth rate is the same for all grains and all directions (i.e. homogeneous and isotropic growth); growth ceases for each grain when it comes into contact with a neighbouring grain. Such a tessellation generates a subdivision of a space into an array of non-overlapping convex polyhedra filling the space. The topology of such an arrangement of grains is equivalent to a fully dense microstructure of a single-phase alloy; each face is shared by two grains, each edge is shared by three grains and each vertex is shared by four grains [56, 57]. The distributions of the number of faces, volumes and surface areas for the three-dimensional Poisson–Voronoi cells are accurately described by a two-parameter gamma distribution [55] with the mean values corresponding to the experimental observations [56–59]. Also, the mean values of dihedral angles (angle between adjacent faces) and bond angles (angles between adjacent edges) are very close to those required by the equilibrium surface tension criteria [60]. Two types of Alloy 600 microstructure were simulated; one composed of 250 grains, the other one composed of 500 grains. Fig. 1 shows a micrograph of an actual microstructure of Alloy 600 and a cross-section of the simulated microstructures.

2.2. Finite element modelling

The Poisson–Voronoi tessellations were generated within a unit cube (Fig. 2) following the algorithms

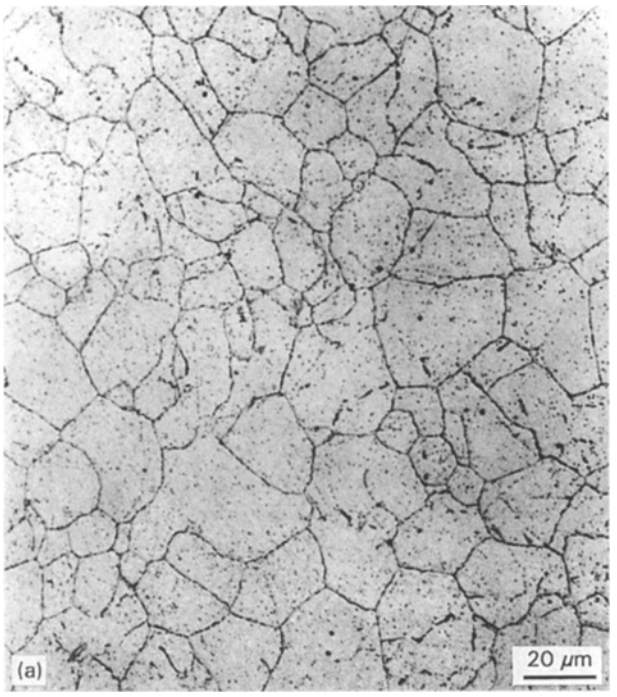

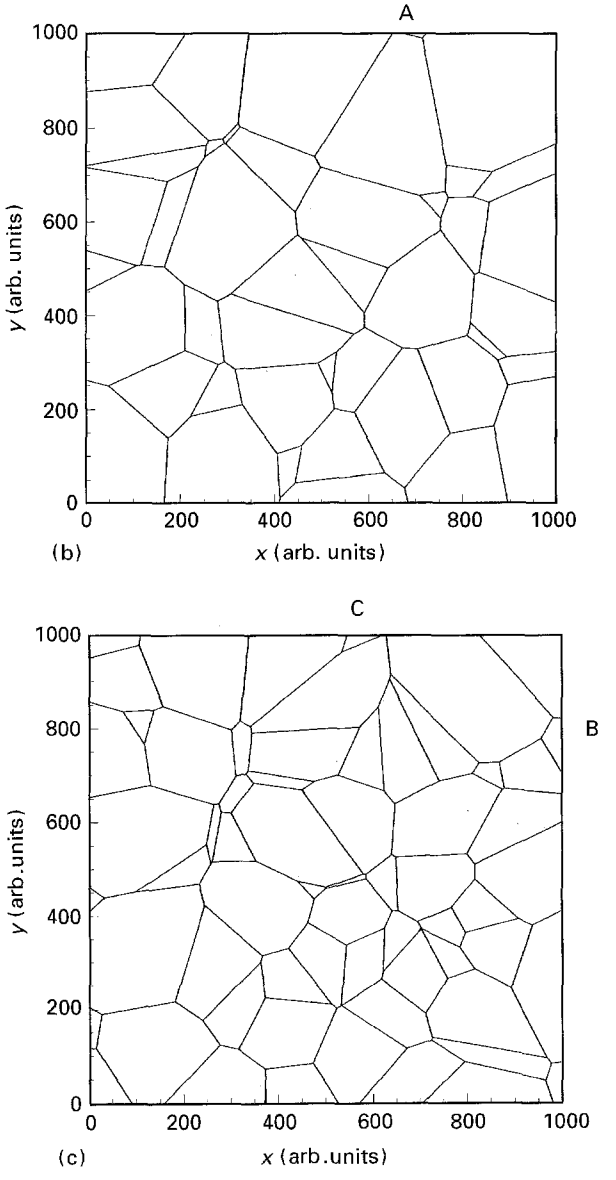

Figure 1 (a) Microstructures of mill-annealed Alloy 600 (after [80]) and computer-simulated microstructures: (b) 250 grains and (c) 500 grains.

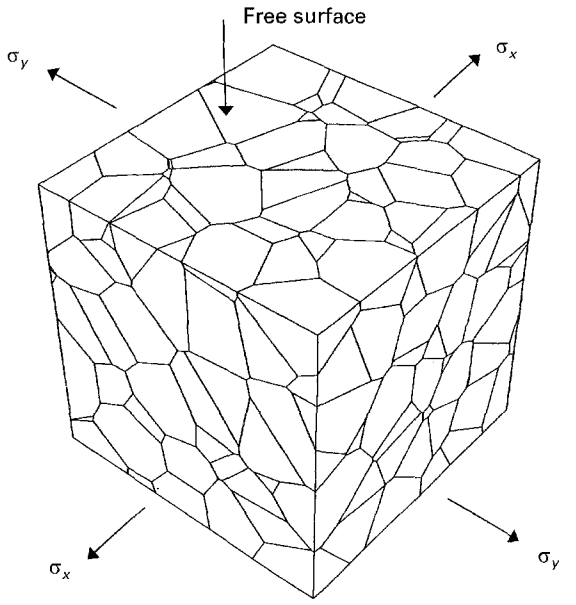

Figure 2 Unit cube showing grain boundaries and loading conditions.

described elsewhere [61]; the simulated microstructures contained 250 grains and 500 grains. They can be interpreted as two microstructures having the ratio of the mean grain sizes approximately equal to 1.25. Such a cube also represents the material surface layer with the thickness of several grains. Each grain was divided into tetrahedral elements having a common vertex at the location of the original seed from which the grain had been grown. Such a division provided for 40–50 finite elements per grain [61].

The simulated microstructures had a random orientation of grains (i.e. no crystallographic texture), that is the single-crystal elastic constants were expressed in a local coordinate system randomly oriented with respect to the sample (global) coordinate system. Each set of random orientations were generated according to the algorithm presented in the Appendix. Because the single-crystal elastic constants for Alloy 600 were not available in the literature, they were estimated from the polycrystal elastic modulus reported elsewhere [62, 63] ($E = 203.6$ GPa). The Zener anisotropy factor $A = 2C_{44}/(C_{11}-C_{12})$ for Alloy 600 was assumed to be equal to the average of the anisotropy factors for nickel and nickel superalloys René N4 [64] and MAR–M200 [64, 65]. The numerical value of $A = 2.76$ was derived for Alloy 600 and the following single-crystal elastic constants were recalculated using the Kröner monocrystal–polycrystal relationship [66]: $C_{11} = 232$ GPa, $C_{12} = 148.0$ GPa, and $C_{44} = 115.9$ GPa. The polycrystal elastic moduli for Alloy 600 estimated by Kröner's [66] averaging scheme were: Young's modulus $E = 203.9$ GPa, shear modulus $G = 78.0$ GPa, bulk modulus $K = 176.0$ GPa, and the Poisson ratio $\nu = 0.307$. The elastic moduli derived using the three-dimensional microstructural model and simulating uniaxial tensile and hydrostatic compression tests were $E = 206.2$ GPa and $K = 176.0$ GPa, showing an excellent agreement with the analytical predictions. The temperature dependence of elastic constants was

not considered because there were no available data; limited experimental evidence shows that at 320 °C (which is the operational regime for Alloy 600 tubing in nuclear power steam generators) the Young's modulus is lower by approximately 10% than the value at room temperature. Also, because Alloy 600 has a cubic structure, there is no thermal anisotropy.

The boundary conditions were established in the following way. Recognizing that an IGSCC crack initiates at the surface where a plane state of stress is present, a biaxial pressure uniformly distributed on the cube faces was applied (Fig. 2). The two unloaded surfaces remained free. The analysis of residual stresses in Alloy 600 components (residual stresses are much higher than applied stresses) [67, 68] showed that two cases of stress state can be considered as "typical": biaxial stress $\sigma_x = \sigma_y$ and $\sigma_y = 0.02\ \sigma_x$ ("almost" uniaxial tension). The numerical values were set as $\sigma_x = 300$ MPa, $\sigma_y = -300$ MPa in the first case and $\sigma_x = 500$ MPa, $\sigma_y = -10$ MPa in the second case, so that the average macroscopic von Mises stress was the same in both cases and equal to $\sigma_m = 505$ MPa (which is approximately 70% of the tensile strength of a mill-annealed Alloy 600 [9]). Such boundary conditions are also interesting from the theoretical standpoint, in that they allowed for the analysis of the stress distribution as a function of loading conditions, i.e. biaxial versus uniaxial stress state. The stresses (von Mises, hydrostatic) at the vertices where the grains meet (four grains meet at a common vertex in the bulk material, three grains meet at the surface) were calculated using MSC/NASTRAN V.66 finite element package as follows

$$\sigma_g = \sum_{e=1}^{N_e} W_{ge}\,\sigma_{ge} \tag{1}$$

where σ_{ge}, an element corner stress component, is multiplied by W_{ge}, the interpolation factor, and summed for all elements, N_e, connected to the vertex.

3. Grain-boundary disorientation angle distribution

A single-phase crystalline material is an aggregate of single crystals (crystallites) which have different orientations in space. In order to characterize quantitatively a grain boundary (an interface between grains), one needs to analyse a general bicrystal. A bicrystal system has five degrees of freedom, i.e. five parameters are necessary to describe it mathematically [69, 70]. The amount of misorientation or the angles necessary to rotate the coordinate system of one crystal so that it coincides with the coordinate system of the other one is described by three independent variables (e.g. three Eulerian angles or 3×3 matrix of cosines between the two coordinate systems). The direction of the grain boundary is described by the directional cosines of a unit vector normal to the grain boundary. In a general sense, all five parameters need to be specified to describe a grain boundary. In material science, however, the misorientation angle is often used as a measure of the misorientation of the crystallographic lattices. If A_1 and A_2 are the orthonormal orientation matrices of two grains creating a grain boundary, the misorientation matrix $R\{r_{ij}\}$ where $i, j = 1, 2, 3$ is given as

$$R = A_1 A_2^{-1} \tag{2}$$

The angle and the vector of misorientation are given as

$$\omega = \arccos \tfrac{1}{2}(Tr\,R - 1) \tag{3}$$

where Tr is trace of matrix,

$$[pqr] = \frac{1}{2 \sin\omega}[r_{32} - r_{23},\ r_{13} - r_{31},\ r_{21} - r_{12}] \tag{4}$$

The misorientation matrices A_i (and, therefore, misorientation angles) cannot be determined unambiguously. For each pair of grains, there are n different but crystallographically equivalent matrices R and angles ω, where n is the number of elements of the proper rotation symmetry group of a crystal ($n = 24$ for a f c c crystal such as Alloy 600).

The disorientation angle is defined as the smallest one from the set of all crystallographically equivalent ones. The maximum value of the angle of disorientation is 2 arc cos $1/4\ (2 + 2^{1/2}) = 62.8°$ which corresponds to the rotation of 90° about any of the axes $\langle 1\,1\,0 \rangle$ of a cubic crystal [71]. The distribution of disorientation angles in a random aggregate of cubic crystals was treated theoretically elsewhere [71, 72]. The density function of disorientation angles calculated for 250 and 500 grains is shown in Fig. 3 together with the Mackenzie's [72] analytical predictions. The agreement with the analytical prediction improves as the population of grains increases. The effect of the surface grain fraction (approximately 60% for the case of 250 grains, and approximately 58% for 500 grains) is small, which is in accordance with the results of Garbacz and Grabski [73], who found no significant effect of surface grain fraction on the distribution of the disorientation angle for an aggregate of 4000 K tetrakaidekahedra. The agreement of the distribution of disorientation angles with the analytical prediction shows that the Poisson–Voronoi tessellation, for which each grain has the orientation assigned randomly using the procedure described in the previous section, represents a random polycrystal.

4. Distribution of stresses in a polycrystalline aggregate

The stresses were calculated at vertices where four grains meet (three grains at the surface) and in the grain interiors at the points corresponding to the location of the original "seeds". Two scalar stresses were calculated: von Mises stress (second invariant of the deviator stress tensor) as relevant to the slip-type mechanism of crack initiation and hydrostatic stress (one-third of the first invariant of the stress tensor) as relevant to the hydrogen embrittlement type of material damage.

4.1 Disorientation angle–stress relationships

There are six disorientation angles associated with each vertex where four grains meet and three disorientation

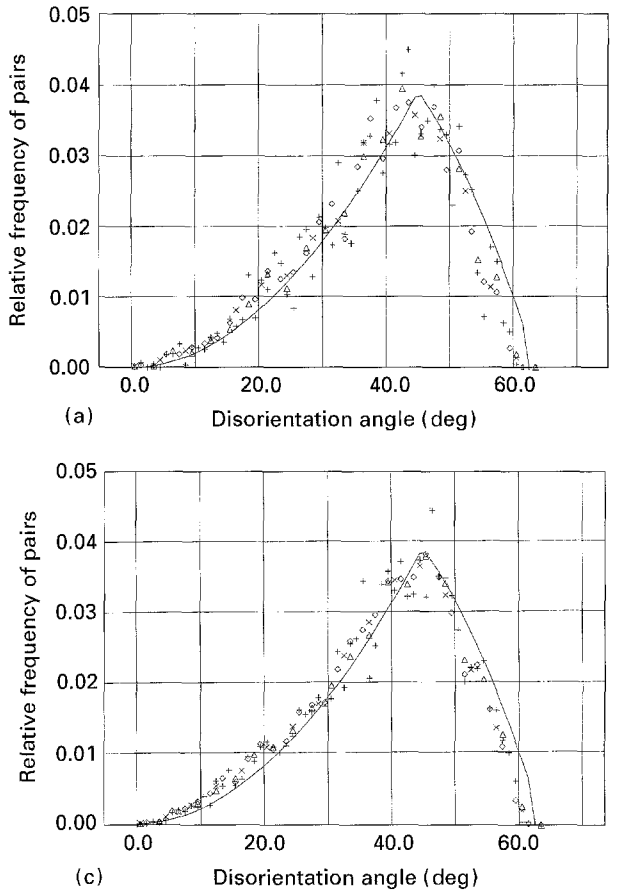

Figure 3 The density function of disorientation angle for (a) 250 grains, first set of orientations, (b) 250 grains, second set of orientations, (c) for 500 grains. (+) average over 1°, (◇) average over 2°, (△) average over 3°, (×) average over 4°, (——) theoretical.

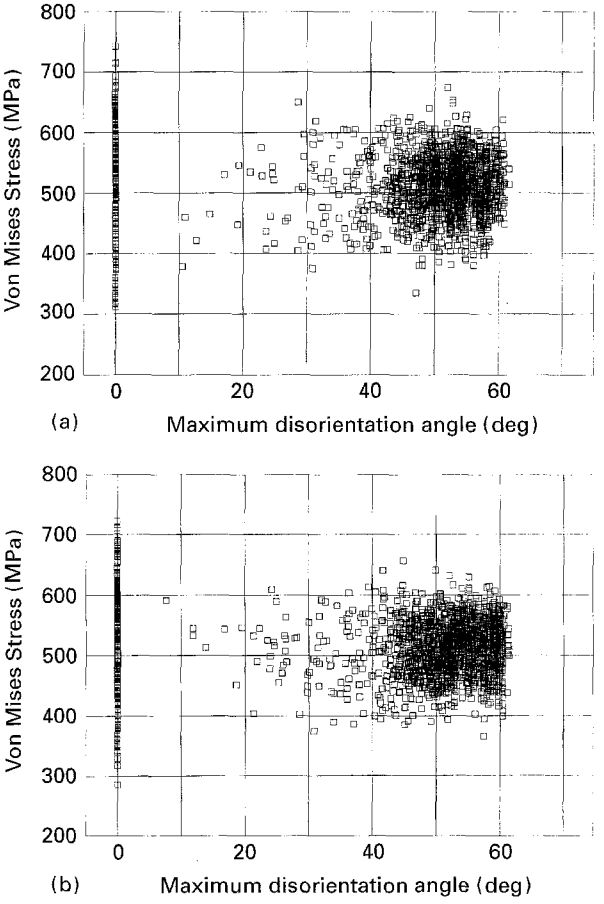

Figure 4 Dependence of von Mises stress on the maximum disorientation angle at vertices and grain "seeds" for 250 grains: (a) first set of grain orientations, (b) second set of grain orientations. Loading conditions for both cases: $\sigma_x = 500$ MPa, $\sigma_y = -10$ MPa.

angles for a grain-boundary triple point on the surface. In order to analyse the relationships between the stresses at the vertices and the misorientation of the grains, three measures of the misorientation were used: maximum, average, and square average of the disorientation angle. Figs 4–7 show the relationships between the maximum disorientation angle and the von Mises and hydrostatic stresses for 250 and 500 grains for different sets of grain orientations and different loading conditions. Figs 4 and 5 show that the character of the von Mises and hydrostatic stress distributions does not depend on the set of random orientations assigned to the grains. However, the local stresses are sensitive to grain orientation. There is no simple relationship between the magnitude of the stress and the maximum disorientation angle (and other measures or misorientation) indicating a strong effect of grain topology i.e. the resultant stress at a vertex is dictated by the interactions with all neighbouring grains, therefore it depends on the grain shape and volume as well as its orientation. Maximum and minimum values of von Mises stress correspond to the grain "seeds" (where the maximum disorientation angle is zero). The concentration of von Mises stresses at the grain seed (defined as the ratio of the maximum stress to the average stress) is approximately 1.54 and the stress concentration at the vertex is approximately 1.49 (Figs 4 and 6). The character of the distribution of von Mises stresses (Fig. 6) is independent of the loading mode (uniaxial versus biaxial in this case); however, the local values of stress, i.e. stresses at particular vertices, vary. This indicates the sensitivity of the local, microscopic stress at the grain-size level to the macroscopic stress tensor. The extreme values of the hydrostatic stress correspond to the vertices where the grains meet, not the grain interiors, as was the case of von Mises stresses (Figs 5 and 7). These extreme values are found for higher maximum disorientation angles; however, the highest disorientation angles do not correspond to the maximum (nor minimum) hydrostatic stresses. The character of the distribution of hydrostatic stresses is insensitive to loading conditions

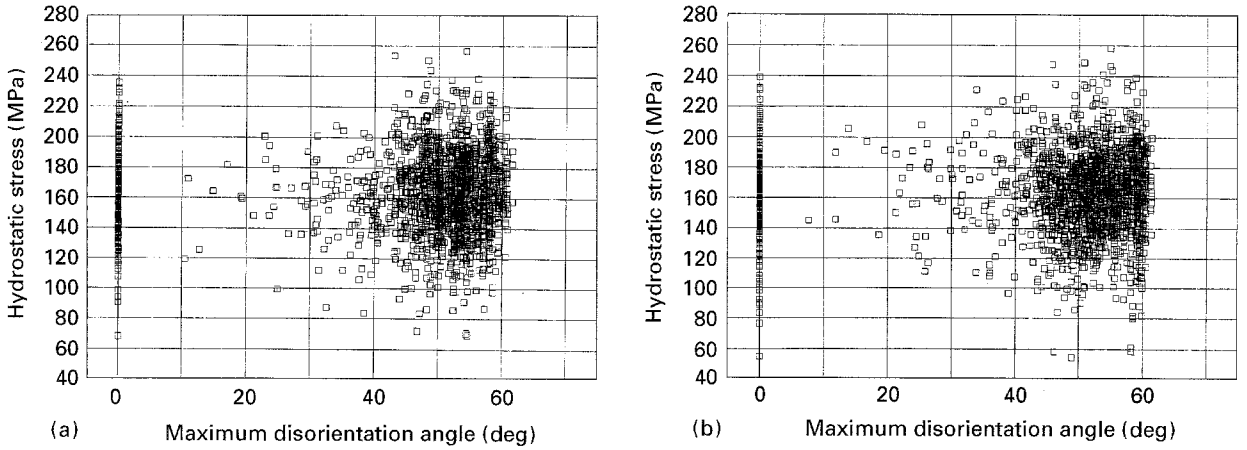

Figure 5 Dependence of hydrostatic stress on the maximum disorientation angle of vertices and grain "seeds" for 250 grains: (a) first set of grain orientations, (b) second set of grain orientations. Loading conditions for both cases: $\sigma_x = 500$ MPa, $\sigma_y = -10$ MPa.

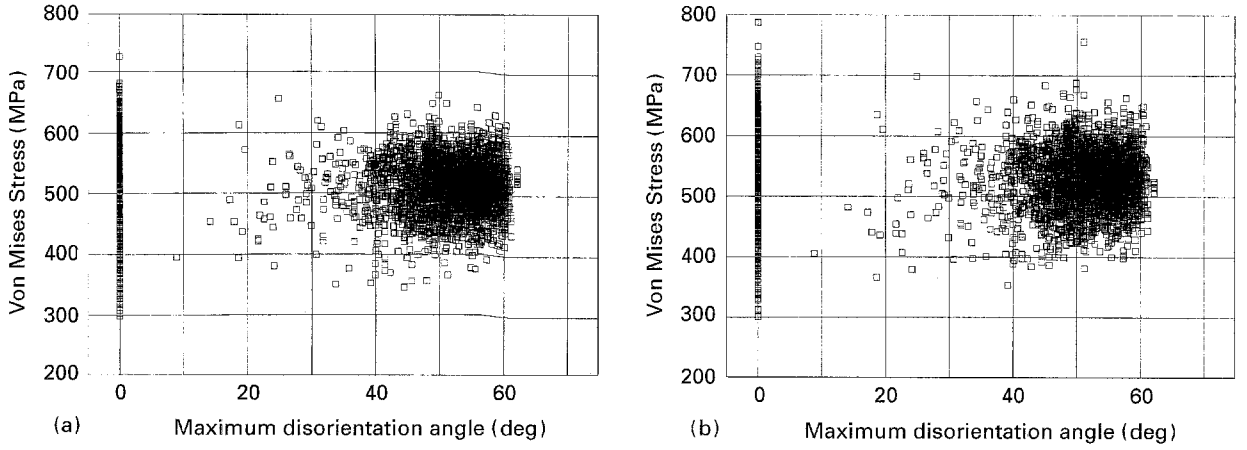

Figure 6 Dependence of von Mises stress on the maximum disorientation angle of vertices and grain "seeds" for 500 grains: (a) loading conditions: $\sigma_x = 500$ MPa, $\sigma_y = -10$ MPa, (b) loading conditions: $\sigma_x = \sigma_y = 300$ MPa.

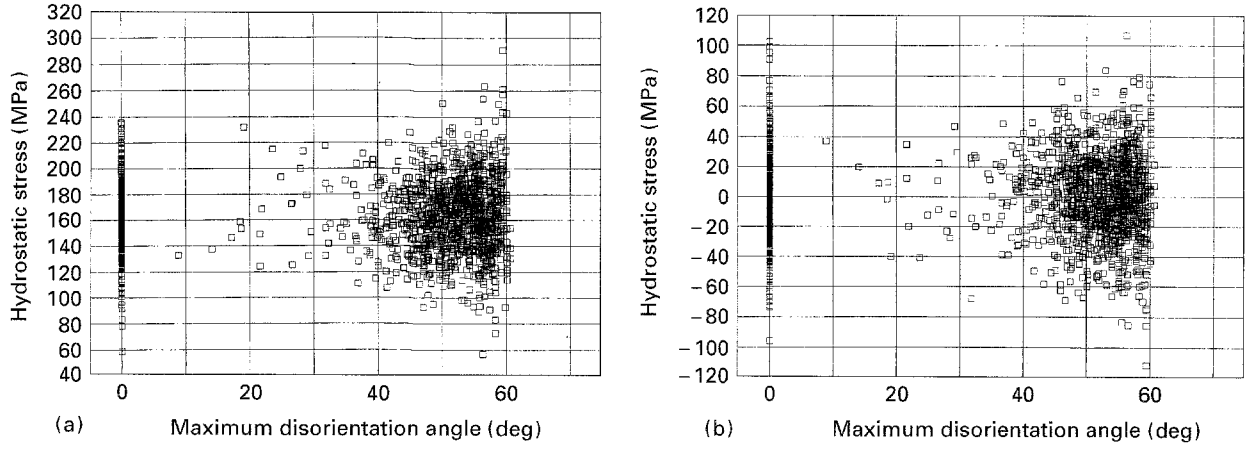

Figure 7 Dependence of hydrostatic stress on the maximum disorientation angle at vertices and grain "seeds" for 500 grains: (a) loading conditions: $\sigma_x = 500$ MPa, $\sigma_y = -10$ MPa, (b) loading conditions: $\sigma_x = -\sigma_y = 300$ MPa.

(Fig. 7), however, the spatial distribution of stresses depends on the applied stress tensor. The maximum hydrostatic stress concentration observed for 500 grains is 1.7 (Fig. 7).

4.2. Stress distribution on a free surface

An example of the stress distribution at the grain-boundary triple points on the free surface as a function of the disorientation angle is shown in Fig. 8. The maximum stress concentration factors were found to be 1.3 for von Mises and 1.6 for hydrostatic stress. Figs 9–12 show the distributions of von Mises and hydrostatic stresses on the free surface and their dependence on the loading mode and grain orientations. Fig. 9 shows that the hydrostatic stress distribution on the surface depends strongly on grain orientations. However, the microstructural features, such as small

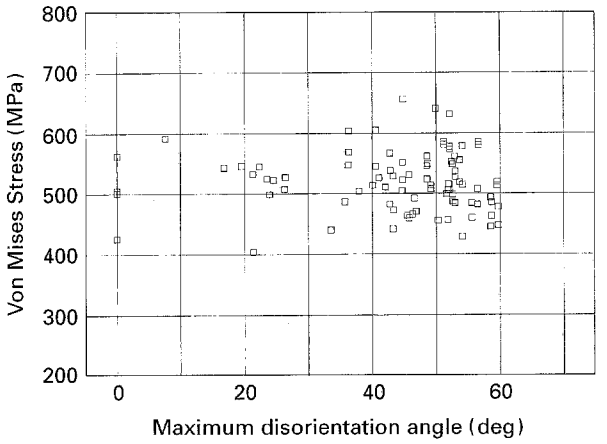

Figure 8 Dependence of von Mises stress on free surface on the maximum disorientation angle for 250 grains (first set of grain orientations). Loading conditions: $\sigma_x = 500$ MPa, $\sigma_y = -10$ MPa.

grains (for example, the grain marked as A in Figs 1 and 9) with sharp shapes, act as stress raisers, regardless of their own orientation and the orientations of the adjacent grains. The same observations apply to von Mises stresses (Fig. 10): stress distribution is dictated by the microstructure (grain topology) and the grain orientations. The effect of loading mode on von Mises stress distribution on the surface is not significant. As seen in Fig. 12, the character of von Mises stress distribution is very similar for the uniaxial and biaxial modes of loading. The distribution of hydrostatic stress is for the most part not strongly dependent on the loading mode (Fig. 11) except for the locations where small grains with irregular shapes (e.g. grains marked as B and C in Figs 1 and 11) act as stress raisers; change of loading from uniaxial to biaxial causes an abrupt change in hydrostatic pressure. Therefore, if the damage criterion based on

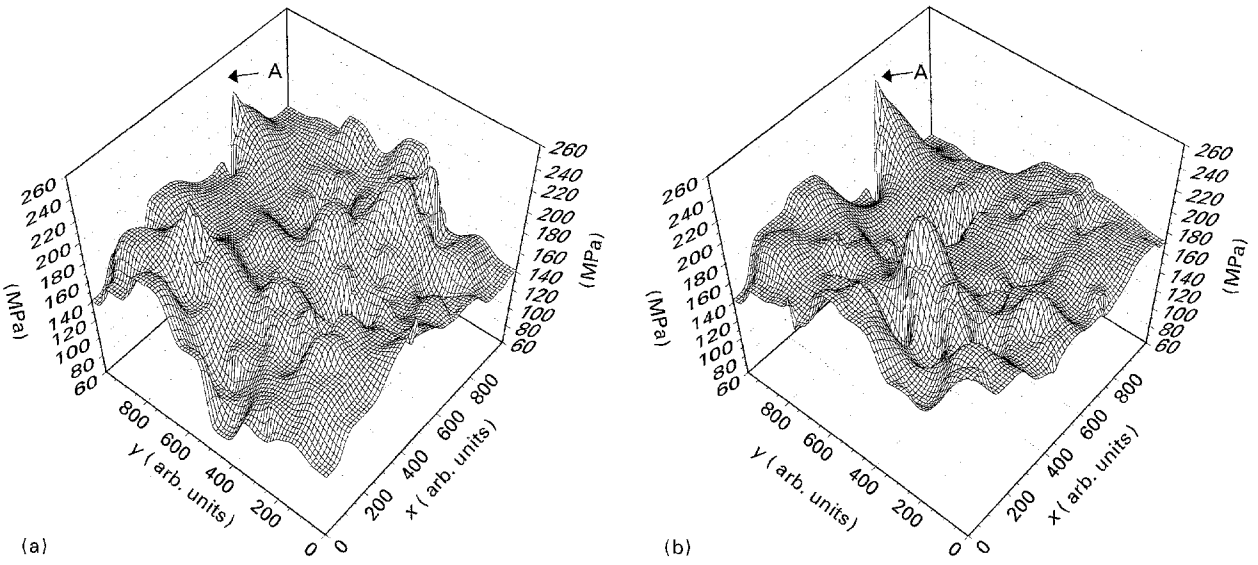

Figure 9 Distribution of hydrostatic stress on the free surface, simulation of 250 grains. Loading conditions: $\sigma_x = 500$ MPa, $\sigma_y = -10$ MPa: (a) first set of grain orientations, (b) second set of grain orientations.

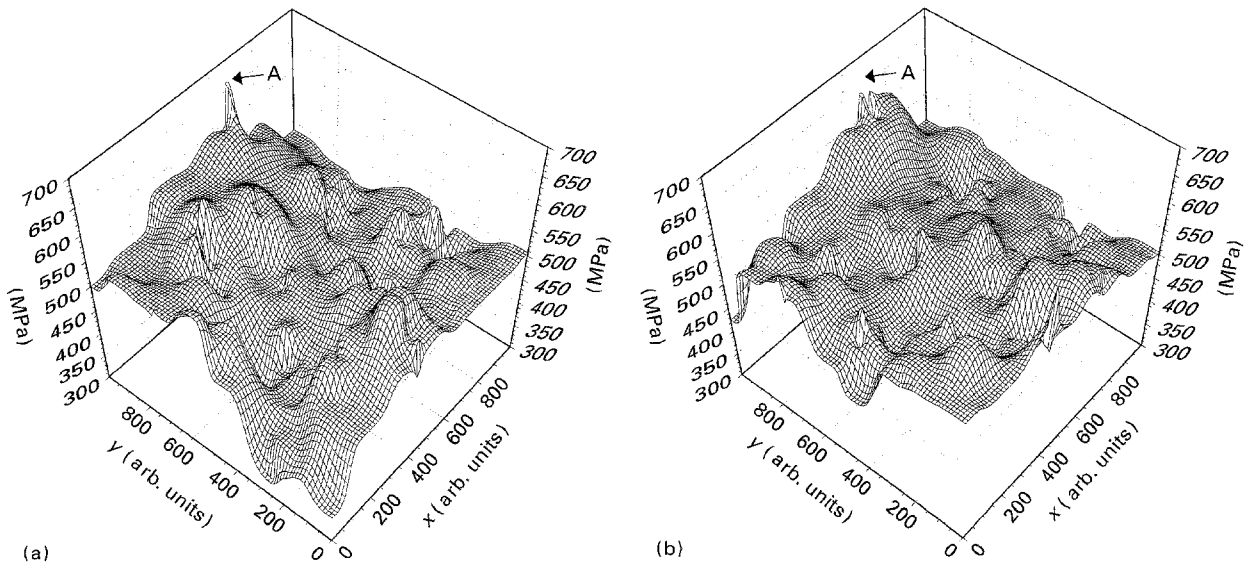

Figure 10 Distribution of von Mises stresses on the free surface, simulation of 500 grains. Loading conditions: (a) $\sigma_x = 500$ MPa, $\sigma_y = -10$ MPa, (b) $\sigma_x = 300$ MPa, $\sigma_y = -300$ MPa.

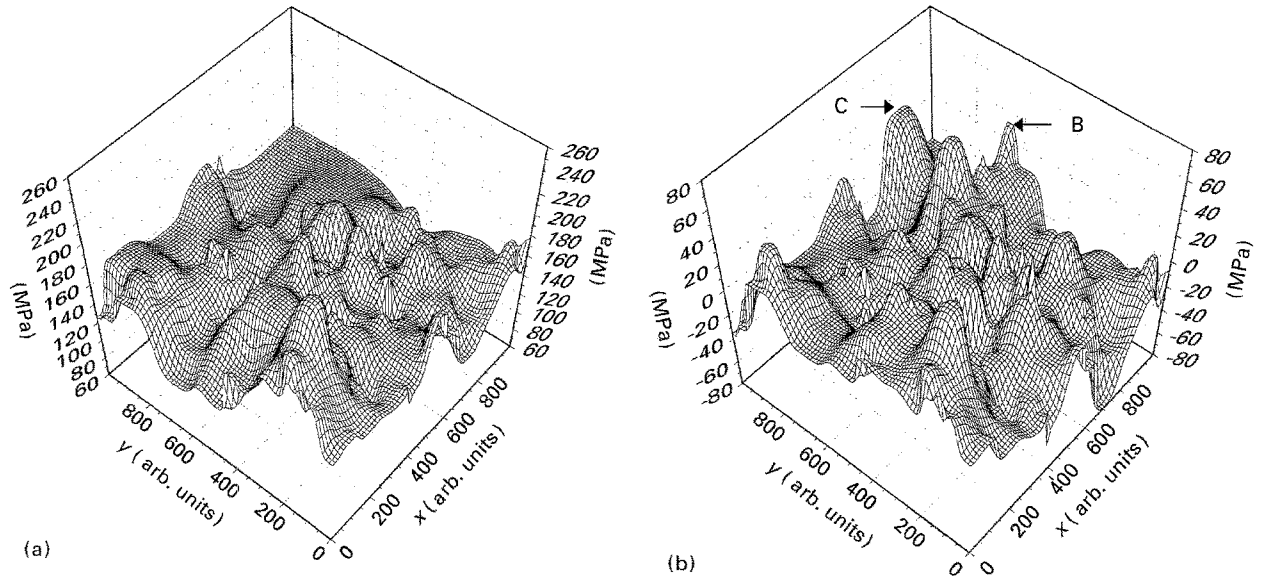

Figure 11 Distribution of hydrostatic stresses on the free surface, simulation of 500 grains. Loading conditions: (a) $\sigma_x = 500$ MPa, $\sigma_y = -10$ MPa, (b) $\sigma_x = 300$ MPa, $\sigma_y = -300$ MPa.

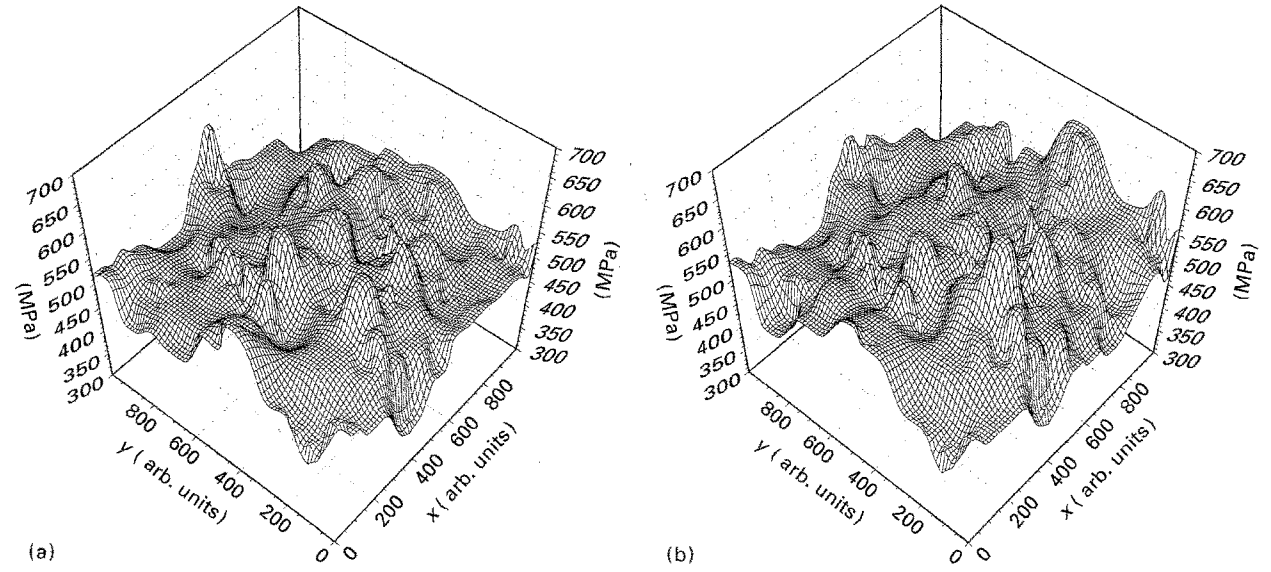

Figure 12 Distribution of von Mises stresses on the free surface, simulation of 500 grains. Loading conditions: (a) $\sigma_x = 500$ MPa, $\sigma_y = -10$ MPa, (b) $\sigma_x = 300$ MPa, $\sigma_y = -300$ MPa.

von Mises or hydrostatic stresses was applicable to Alloy 600, a uniaxial SCC test would not reflect the stress effects due to actual multiaxial loading of a component.

5. Discussion

The effects of crystal anisotropy on the stress distribution have been studied mostly for two-dimensional arrays of hexagonal grains modelling polycrystalline aggregate [74–78]. McKinstry *et al.* [74, 75] studied numerically the effects of anisotropy on the maximum principal shear and normal stress, in an aggregate of 19 hexagonal crystals of alumina. They found that the anisotropic characteristics of the material altered the location where the magnitude of the shear stress was maximum under isostatic, uniaxial, and thermal loadings. Fu and Evans [76] analysed analytically the stress distribution within a grain in a model consisting of four anisotropic hexagonal grains embedded in an isotropic matrix. The residual stress comprised of two principal components: uniform stresses at the grain-facet centre (caused by the thermal mismatch between the two grains adjacent to the grain boundary) and singular stresses near the grain corner. The singular stresses displayed a logarithmic dependence on the distance from the grain corner

$$\sigma_{ij} = \sigma_{ij}^{M}\left(a + b \ln \frac{l}{x}\right) \quad (5)$$

where σ_{ij}^{M} is the uniform stress at the grain-facet centre, l is the grain facet length, x the distance from the grain corner, and a, b are functions of elastic properties and the misorientation between grains. Tvergaard and Hutchinson [77] studied the effect of crystal anisotropy on stress distribution considering a planar array of hexagonal grains as a model of

a polycrystalline ceramic. The stress singularities at triple-grain junctions were studied by an asymptotic method and by a numerical solution. It was found that the nature of the singularity depended on the junction geometry and the elastic anisotropies of the grains; in some cases, the stresses were unbounded, in others the stresses decayed to zero. The numerical solution for a cubic material (whose anisotropy was characterized by two factors: $R = (C_{12} + 2C_{44})/C_{11} = 1.5$ and various ratios of $Q = 2C_{44}/C_{12}$) for some specific arrangement of grain orientations (not random), showed the stress concentration of the normal stress at the triple-grain junction of 1.5. For $R = 0.5$ the stresses decayed to zero at the grain-boundary triple point; Q had less influence on stress distribution. For Alloy 600, $R = 1.64$ and $Q = 4$, which is closer to the first case, i.e. stress concentration factor of 1.5; the stresses interpolated at vertices in this research showed the maximum concentration factors of 1.5 for von Mises and 1.7 for the hydrostatic stresses. The results of Tvergaard and Hutchinson [77] were consistent with the results of Laws and Lee [78], who also confirmed that the stress singularity at a triple point was logarithmic. The analysis of the stress state in a polycrystal by means of contact-problem theory [42] showed that the resultant stress state is a superposition of the homogeneous stress state and contact stresses at the boundaries between misoriented grains. The contact stresses oscillate with increasing amplitude as the distance to the triple point decreases and, depending on the elastic mismatch, can reinforce or counteract the effect of the homogeneous stress. In qualitative terms, the stress tensor along the grain boundary can be expressed as

$$\sigma_{ij} \sim \bar{\sigma}_{ij}\left[A + \mathrm{B}\left(\frac{d}{r}\right)^{1/2}\right] \tag{6}$$

where $\bar{\sigma}_{ij}$ is the average stress along the cross-section, d is the mean grain size, r the distance from the triple point measured along the grain boundary and constants A and B depend on elastic properties and misorientation of adjacent grains. From both Equations 5 and 6 it follows that the stress concentration at triple points for planar hexagonal grains of uniform size depends on the grain size; increase of the mean grain size increases the stress concentration factor. The current research for three-dimensional arrangements of grains having a two parameter gamma distribution of volumes shows that small grains are more effective stress raisers. The stress distribution in a grain results from the interactions with all neighbouring grains (14 on average for a single-phase material); however, the smaller grains have fewer faces (and neighbours) than the bigger ones, with the minimum number of four. Therefore, the effect of the potential extreme contact stresses with one neighbour is more pronounced in the case of small grains.

In general, the stress distribution in a polycrystalline aggregate depends on the grain-size distribution and the grain-boundary misorientation distribution function. Dikusar *et al.* [79] used the theory of random functions to analyse the microdeformation of random polycrystals. The model polycrystal was composed of the uniform size grains and the inhomogeneity of the material resulted from the presence of definite boundaries between the separate crystallites. Assuming the normal distribution density of the grains with respect to stress, i.e. assuming that almost all (i.e. 99.7%) possible values of stress lie in the interval $\sigma \pm 3\,S$, where σ is the external stress averaged over all crystallites and S is the standard deviation proportional to stress

$$S = \sigma\Delta \tag{7}$$

$$\Delta = 0.145\,K|\lambda_6|/(K + 4/3\,G)E \tag{8}$$

where K is the bulk modulus, G the shear modulus, E is Young's modulus, and $\lambda_6 = C_{11}-C_{12}-2C_{44}$; C_{ij} are single-crystal elasticity constants. The term $(1 + 3\Delta)$ represents the stress concentration factor due to the discontinuity of elastic properties across the grain boundary, and for Alloy 600 elastic constants cited in Section 2.2 it is equal to 1.2; the higher values of stress concentration can occur but with much lower probability. The current research shows (e.g. Figs 4–6) that for 97% of vertices the von Mises stresses lie in the region $\pm$ 20% from the average stress; dispersion of hydrostatic stress is approximately $\pm$ 25%. The most probable and extreme values of stresses reported in the present research are in agreement with the analytical and numerical results reported in this section. Higher stress concentration values found in the three-dimensional microstructure can be caused by the lognormal distribution of grain sizes.

6. Conclusion

The stress distribution in a polycrystalline material (Alloy 600) was studied using a topologically correct microstructural model. The distributions of von Mises and hydrostatic stresses, which could be important factors when studying the IGSCC initiation, at the grain vertices, were analysed as a function of microstructure, grain orientations and loading conditions. The grain size, shape, and orientation had a more pronounced effect on stress distribution than the loading conditions. The stress concentration factor was higher for hydrostatic stress (1.7) than for von Mises stress (1.5) for Alloy 600 (Zener anisotropy factor $A = 2.76$); hydrostatic stress showed more pronounced dependence on the disorientation angle than von Mises stress. The observed stress concentration is high enough to cause the localized plastic microdeformation, even when the polycrystalline aggregate is in the macroscopic elastic regime. The modelling of stresses and strains in polycrystalline materials can identify the microstructures (grain-size distributions, texture) intrinsically susceptible to stress/strain concentrations and justify the correctness of applied stress state during the SCC tests.

Acknowledgements

The authors thank Dr H. M. Ledbetter, National Institute of Standards and Technology, Boulder, CO,

for calculating the single-crystal elastic constants of Alloy 600. This project was supported by the Electric Power Research Institute, Palo Alto, CA.

Appendix. Computing components of a random unit vector

The problem of randomly generating the local coordinate systems (grain orientations) expressed in terms of a global coordinate system (fixed to the unit cube) is equivalent to calculating random orthogonal 3×3 matrices whose elements are the directional cosines between the local and global coordinate systems [71]. This problem can be reduced to computing the elements of a random unit vector [1]. The cosine of the angle between a fixed direction and a random direction is uniformly distributed on the range $(-1,1)$. Therefore, if ξ, the cosine of the co-latitude, is chosen at random in the range $(-1,1)$ and the longitude ϕ is chosen at random in the range $(-\pi,\pi)$, the random unit vector is given by

$$[\pm(1-\xi^2)^{1/2}\cos\phi, \pm(1-\xi^2)^{1/2}\sin\phi, \xi] \quad (1)$$

where the $\pm$ sign is assigned randomly.

References

1. G. P. AIREY, *Metallography* **13** (1980) 21.
2. M. KOWAKA, H. NAGANO, T. KUDO, Y. OKADA, M. YAGI, O. TAKABA, T. YONEZAWA and K. ARIOKA, *Nucl. Technol.* **55** (1981) 394.
3. G. P. AIREY and A. R. VAIA, "A Caustic Stress-Corrosion Cracking Evaluation of Thermally Treated Inconel Alloy 600 Steam Generator Tubing, MiCon 82: Optimization of Processing Properties and Service Performance Through Microstructural Control", edited by H. Abrams, E. Clark, J. Hood and B. Seth (American Society for Testing and Materials, Philadephia, PA 1982) p. 59.
4. S. M. BRUEMMER and C. H. HENAGER Jr, in "Proceedings of the 2nd International Symposium on Environmental Degradation of Materials in Nuclear Power Systems – Water Reactors", National Association of Corrosion Engineers, Houston, TX, 1985 (American Nuclear Society, Lagrange Park, IL, 1986) p. 293.
5. *Idem, Scripta Metall.* **20** (1986) 909.
6. S. M. BRUEMMER, L. A. CHARLOT and C. H. HENAGER Jr, *Corrosion* **44** (1988) 782.
7. J. J. KAI, C. H. TSAI, T. A. HUANG and M. N. LIU, *Metall. Trans.* **20A** (1989) 1077.
8. G. S. WAS, *Corrosion* **46** (1990) 319.
9. C. FUNG LO, H. KAMIDE, W.E. MAYO, S. WEISSMANN, EPRI report NP-6705-SD, "Measurement of Surface-Induced Microplasticity in Alloy 600 C-Rings" (EPRI, Palo Alto, CA, 1990) p. 2.
10. J. K. SUNG and G. S. WAS, *Corrosion* **47** (1991) 824.
11. G. S. WAS, J. K. SUNG and T. M. ANGELU, *Metall. Trans.* **23A** (1992) 3343.
12. J. K. SUNG, J. KOCH, T. ANGELU and G. S. WAS, *ibid.* **23A** (1992) 2887.
13. J. KÜPPER-FESER and H. J. GRABKE, *Mater. Sci. Technol.* **7** (1991) 111.
14. J. J. KAI, G. P. YU, C. H. TSAI, M. N. LIU and S. C. YAO, *Metall. Trans.* **20A** (1989) 2057.
15. R. BANDY and D. VAN ROOYEN, *Corrosion* **40** (1984) 281.
16. G.-P. YU and H.-C. YAO, *ibid.* **46** (1990) 391.
17. P. G. CACERES, B. RALPH, G. C. ALLEN and R. K. WILD, *Philos Mag. A* **59** (1989) 1119.
18. *Idem, ibid.* **59** (1989) 1137.
19. *Idem, Surf. Interface Anal.* **12** (1988) 191.
20. N. TOTSUKO, E. LUNARSKA, G. CRAGNOLINO and Z. SZKLARSKA-SMIALOWSKA, *Corrosion* **43** (1987) 505.
21. T. S. BULISCHECK and D. VAN ROOYEN, *ibid.* **37** (1981) 597.
22. D. C. CRAWFORD and G. S. WAS, *Metall. Trans.* **23A** (1992) 1195.
23. T. WATANABE, *Mater. Forum* **11** (1988) 284.
24. M. YAMASHITA and T. MIMAKI, *Philos. Mag. A* **63** 4 (1991) 695.
25. G. PALUMBO and K. R. AUST, *Acta Metall. Mater.* **38** (1990) 2343.
26. T. WATANABE, M. TAKAZAWA and H. OIKAWA, in "Strength of Metals and Alloys" (ICSMA8), edited by P. O. Kettunen, T. K. Lepistö, and M. E. Lehtonen (Pergamon Press, Oxford, 1988) p. 1357.
27. J. YAMASHITA and T. MIMAKI, *Scripta Metall.* **22** (1988) 1087.
28. H. VEHOFF, H. STENZEL and P. NEUMANN, *Z. Metall kde* **78** (1987) 550.
29. T. S. BULISCHECK and D. VAN ROOYEN, *Nucl. Technol.* **55** (1981) 383.
30. P. L. ANDRESEN and F. P. FORD, *Mater. Sci. Eng.* **A103** (1988) 167.
31. R. BANDY and D. VAN ROOYEN, *J. Mater. Energy Systems* **7** (1985) 237.
32. Y. S. GARUD and A. R. McILREE, *Corrosion* **42** (1986) 99.
33. P. R. SWANN and J. D. EMBURY, In "High-Strength Materials", edited by V. F. Zackay (Wiley, New York, 1964) p. 327.
34. D. A. VERMILYEA, in Proceedings of Conference Stress Corrosion Cracking and Hydrogen Embrittlement of Iron Base Alloys, Unieusc-Firminy, France, 12–16 June 1972 edited by R. W. Stachle, J. Hockmann, R. D. McCright and J. E. Slater (National Association of Corrosion Engineers, Houston, TX, 1977) p. 208
35. E. N. PUGH, *ibid.* p. 37.
36. T. MAGUIN, in "Corrosion-Deformation-Interactions CDI '92", 5–7 October 1992, Fontainbleau, France, to be published.
37. C. H. SHEN and P. G. SHEWMON, *Metall. Trans.* **21A** (1990) 1261.
38. *Idem, Corrosion* **47** (1991) 1857.
39. P. M. SCOTT and M. LE CALVAR, EPRI Alloy 600 Expert Meeting, Airlie, VA, 6–9 April 1993 edited by A. R. McIlree, to be published.
40. R. N. PARKINS, *J. of Met* (1992) 12.
41. P. COMBRADE, EPRI Alloy 600 Expert Meeting, Arilie, VA, 6–9 April 1993 edited by A. R. McIlree, to be published.
42. YU. V. GRINYAER and V. E. PANIN, *Izv. Vyss. Uchebn. Zaved. Fizi* **12** (1978) 95.
43. K. HASHIMOTO and H. MARGOLIN, *Acta Metall.* **31** (1983) 773.
44. *Idem, ibid.* **31** (1983) 787.
45. V. E. PANIN, YU. V. GRINYAER, T. F. ELSUKOVA, K. P. ZHUKOVA and E. M. NOVOSELOVA, *Sov. Phys. Dokl.* **34** (1989) 1034.
46. P. VAN HOUTTE and L. DE BUYSER, *Acta Metall. Mater.* **41** (1993) 323.
47. A. K. HEAD, *Aust. J. Phys.* **13** (1960) 613.
48. T. E. MITCHELL, *Philos. Mag.* **10** (1964) 301.
49. Z. S. BASINSKI and T. E. MITCHELL, *ibid.* **11** (1965) 103.
50. I. H. LIU and R. THOMSON, *Acta Metall. Mater.* **34** (1986) 187.
51. M. YAMASHITA and T. MIMAKI, *Philos. Mag.* **A63** (1991) 707.
52. A. GARBACZ and M. W. GRABSKI, *Scripta Metall.* **23** (1989) 1369.
53. V. V. RYBIN, YU. F. TITOVETS, D. M. TEPLITSKIY and N. YU. ZOLOTEREVSKIY, *Phys. Met. Metall.* **53** (1982) 122.
54. V. YU. GERTSMAN, A. P. ZHILYAEV, A. I. PSHENICHNYUK and R. Z. VALIEV, *Acta Metall. Mater.* **40** (1992) 1433.
55. S. KUMAR, S. K. KURTZ, J. R. BANAVAR and M. G. SHARMA, *J. Stat. Phys.* **67** (1992) 523.
56. C. S. SMITH, "A Search for Structure" (MIT Press, Cambridge, MA, 1981).

57. F. N. RHINES and K. R. CRAIG, *Metall. Trans.* **5** (1974) 413.
58. S. K. KURTZ and F. M. A. CARPAY, *J. Appl. Phys.* **51** (1980) 5725.
59. *Idem, ibid.* **51** (1980) 5745.
60. S. KUMAR and S. K. KURTZ, *Mater. Charact.* in press.
61. S. KUMAR PhD thesis, Pennsylvania State University (1992).
62. W. WESTON, H. LEDBETTER and E. NAIMON, *Mater. Sci. Eng.* **20** (1975) 185.
63. S. G. EPSTEIN and O. N. CARLSON, *Acta Metall.* **13** (1965) 487.
64. D. DANDEKAR and A. MARTIN, *J. Mater. Sci. Lett.* **8** (1989) 1172.
65. H. A. KUHN and H. G. SOCKEL, *Phys. Status Solidi (a)* **110** (1988) 449.
66. E. KRÖNER, *Z. Phys.* **151** (1958) 504.
67. C. O. RUUD *et al.*, "Residual Stress Analysis of Alloy 600 U-Bends, RUBs, and C-Rings", EPRI Report TO-104340 (EPRI, Palo Alto, CA, 1994).
68. C. O. RUUD and M. E. JACOBS, "Residual Stresses in Roller Expanded Heat Exchanger Tube Transitions", EPRI Report TR-102355 (EPRI, Palo Alto, CA, 1993).
69. F. F. LANGE, *Acta Metall.* **15** (1967) 311.
70. H.-J. BUNGE, "Texture Analysis in Materials Science" (Butterworths, London, 1982) p. 281.
71. J. K. MACKENZIE and M. J. THOMSON, *Biometrika* **44** (1957) 205.
72. J. K. MACKENZIE, *ibid.* **45** (1958) 229.
73. A. GARBACZ and M. W. GRABSKI, *Acta Metall. Mater.* **41** (1993) 469.
74. H. A. MCKINSTRY, H. E. SHULL and W. R. BUESSEM, *Nucl. Metall.* **20** (1976) 695.
75. *Idem, ibid.* **20** (1976) 929.
76. Y. FU and A. G. EVANS, *Acta Metall.* **33** (1985) 1515.
77. V. TVERGAARD and J. W. HUTCHINSON, *J. Am. Ceram. Soc.* **71** (1988) 157.
78. N. LAWS and J. G. LEE, *J. Mech. Phys. Solids* **37** (1989) 603.
79. L. D. DIKUSAR, E. F. DUDAREV and V. E. PANIN, *Izv. Vyssh. Uchebn. Zaved. Fiz.* **8** (1971) 96.
80. R. C. BALLINGER, R. M. LATANISON, W. C. MOSHIER and R. M. PELLOUX, "The Effects of Heat Treatment on Corrosion Fatigue", EPRI Report TR-102436 (EPRI, Palo Alto, CA, 1993).

Received 14 September 1993
and accepted 27 September 1994